Cement and Concrete Composites 157 (2025) 105894

Contents lists available at ScienceDirect

Cement and Concrete Composites

journal homepage: www.elsevier.com/locate/cemconcomp

Boosting cement hydration with boron nitride nanotubes

Chandrasekhar Bhojaraju [a], Claudiane M. Ouellet-Plamondon [b,*]

[a] St Joseph Engineering College, Vamanjoor, Mangalore, 575028, India
[b] École de technologie supérieure, Université du Québec, Montreal, H3C 1K3, Canada

ARTICLE INFO

Keywords:
Cement
Boron nitride nanotubes
Graphene
Graphene oxide
Hydration
Nanomaterials

ABSTRACT

In recent years, there has been a growing interest in the use of nanomaterials as additives in various industries, including cement production. Among these materials, carbon-based nanomaterials, such as graphene and graphene oxide, have been extensively studied for their potential applications in cementitious materials. However, recent research has shown that boron nitride nanotubes (BNNT) can offer superior properties compared to their carbon-based counterparts. This study compared the properties of BNNT with those of graphene and graphene oxide when used as additives in cementitious materials. The hydration process of the nanomodified cementitious composite was studied using in situ calorimetry measurements over a period of seven days, and thermogravimetric analysis (TGA), X-ray diffraction (XRD), Fourier-transform infrared spectroscopy (FTIR), nuclear magnetic resonance (NMR), and Field Emission Scanning Electron Microscopy (FESEM) over a period of 28 days. These techniques provide insights into the mechanisms of cement hydration and the impact of boron nitride nanotubes on cementitious composites. The results demonstrate that the addition of BNNT significantly reduced the induction period during cement hydration, indicating that BNNT can enhance the reactivity of cement. Furthermore, BNNT accelerate the hydration process because of their high surface area. Phase identification by XRD peaks showed that the BNNT reinforcement could regulate the microstructure of the cementitious composites. These findings suggest that BNNT has the potential to be a more effective and efficient additive in cementitious materials than graphene and graphene oxide. The use of BNNT in cement production can lead to the development of high-performance, durable, and sustainable materials for various construction applications.

1. Introduction

Cement production is a recognized cause of anthropogenic global warming. Cement improvement and breakthrough technologies, including the potential use of nanomaterials, are among the proposed solutions [1]. However, the proficiency of nanomaterials to enhance cement hydration has not yet been clearly established. A significant improvement with nano admixtures can potentially reduce the amount of cement in concrete. However, owing to their strong agglomeration tendency, obtaining homogeneous nano dispersions is extremely challenging, which is a prerequisite for successfully utilizing nanomaterials in most applications, including composite materials [2]. Comprehensive characterization at the multiscale level is essential to truly understand and harness the benefits of nanomaterials for cement improvement. The full characterization of calcium silicate hydrate (C-S-H) requires a multiscale analysis. The C-S-H is the gel that binds the cement phases together, and it is heterogeneous and nanoporous. The disordered stacked sheets of calcium and oxygen atoms and silicate tetrahedra are separated by sheets of water with nano-sized gel pores and larger capillary pores [2]. Nuclear magnetic resonance (NMR) analysis is usually required to investigate the nanospheres of cement [3].

Graphene (G) and graphene oxide (GO) have excellent potential as reinforcing materials for high-performance composites, based on the effect they have on cement hydration [4,5]. These materials contribute to enhancing the toughness of cementitious composites. The limitation of these carbon based nanomaterials is that they accelerate corrosion in blends without a high proportion of slag [6]. Thus, other nanomaterials merit further investigation. Nanoparticles prevent the formation and propagation of microcracks, as well as contribute to the improvement of the densification of matrix [7]. Among the promising nanomaterials being explored, boron nitride nanotubes (BNNT) have emerged as a particularly intriguing option for enhancing cementitious composites. BNNT have groundbreaking improvements in material sciences. Nanosheets of boron nitride are 2D nanomaterials that have been extensively exfoliated and used as reinforcements in composite materials. BNNT has superior chemical stability, mechanical strength, and thermal

* Corresponding author.
E-mail address: claudiane.ouellet-plamondon@etsmtl.ca (C.M. Ouellet-Plamondon).

https://doi.org/10.1016/j.cemconcomp.2024.105894
Received 22 October 2023; Received in revised form 22 September 2024; Accepted 11 December 2024
Available online 18 December 2024

conductivity compared with carbon nanotubes [8,9]. BNNT exhibits superior mechanical strength and stiffness, which remain largely unchanged even as the number of layers increases. In contrast, G experiences a significant drop in strength (up to 30 %) as the number of layers increases from 1 to 8 [10]. The superior interlayer integrity of BNNTs ensures that their exceptional mechanical properties are maintained, making them highly effective for improving the strength and toughness of cementitious materials. Furthermore, the larger surface area of BNNT (2600 m^2/g) [10,11] results in more robust interfacial interactions with the cement matrix when compared to low-dimensional nanomaterials, including G and GO [11,12]. This provides more nucleation sites for the hydration products. BNNTs are chemically inert and resistant to most acids, bases, and organic solvents, ensuring their long-term durability in the highly alkaline environment of cementitious materials [13]. They exhibit exceptional thermal stability and can resist oxidation up to temperatures of approximately 800 °C [14], making them suitable for applications involving high temperatures or fire resistance. Unlike carbon-based nanomaterials, BNNTs are unaffected by the alkaline environment of cement [15], which reduces the risk of degradation or adverse interactions. This ensures that their reinforcing effect is maintained over time, contributing to the long-term performance of cementitious composites. The unique combination of superior mechanical properties, chemical stability, and high surface area of BNNT provides a promising opportunity to develop high-performance cementitious composites. BNNT has already shown promise in increasing the biocompatibility of dental cements [9], dental adhesives [16], and regenerative medicines [8] and have an effect on oil absorption [17]. Despite these promising properties, the mechanisms underlying the enhancement of cementitious composites by BNNTs have not yet been fully elucidated. Details of the interactions between BNNTs and cement paste cannot be obtained solely from macroscopic investigations [18].

The main objective of this study was to compare the effects of BNNT, G, and GO on the hydration process and microstructure development of cementitious materials, with emphasis on their hydration enhancement capabilities. By conducting this comparative analysis, we aim to contribute to the field of construction materials by describing the mechanism by which these nanomaterials influence cement hydration kinetics and quantifying and qualifying changes in the cement microstructure, which aids in developing high-performance cement. To accomplish these goals, an in-depth analysis of the cementitious microstructure was conducted using isothermal calorimetry to quantify parameters such as heat evolution, induction, and acceleration period and to analyze the degree of hydration and the formation of hydration products through thermogravimetric analysis (TGA) and X-ray diffraction (XRD). In addition to examining the nanostructure of the C-S-H gel, solid-state Nuclear Magnetic Resonance (NMR) spectroscopy was used, focusing on the changes in the C-S-H chain length and connectivity.

2. Materials and methods

2.1. Materials

In this study, general use Portland cement (GU, type-1) was chosen to prepare the cement paste. A polycarboxylate ether (PCE)-based superplasticizer (SP) was used at a constant dosage of 1 % by weight of cement in all mixes. Graphene Black 3X(G) nanoparticles were procured from Nano Xplore. To achieve uniform dispersion, 10 g of G powder was exfoliated in 1 L of distilled water and sodium cholate (1:5 ratio). This mixture was processed using a high-speed shear mixer at 5000 rpm for 1 h [19]. The G used contained 91 % carbon (C), 7 % oxygen (O), 0.5 % sulfur (S), and 2 % other elements, with an average particle size of 40 μm. GO supplied by Graphenea Inc., Cambridge, USA, was used in this study. GO was received in the form of dispersion in water at 4 mg/mL. GO consists of 49–56 % C, 41–50 % O, 2–4% S, and 0–2% other elements with a particle size of less than 7 μm. For the GO dispersion, 75 ml of the GO solution was measured and sonicated with 5 g of superplasticizer (SP) for 30 min using a 40 kHz bath sonicator. This sonicated GO-SP mixture was then incorporated into the cementitious composite, and the amount of SP used for sonication was deducted from the total SP dosage to maintain consistency across all mixes [20]. BNNT were obtained from BNNT Ltd., U.S. The BNNTs had a BN content greater than 99 % (refined materials), with residual impurities of <1 wt % elemental boron, low tap density of ~0.25 mg/cm^3 with extremely low defect density. The surface area of BNNT is up to 400 m^2/g and has a network of many isolated tubes and bundles up to 5 tubes, typically with 1–5 walls (2 or 3 most common), and lengths up to 200 μm with longer tubes suspected. The properties of nanomaterials are presented in Table 1.

For better dispersion of BNNT, 0.3 g of BNNT was initially made into a paste using 10 mL of ammonium oleate surfactant with a mortar and pestle, and an additional 90 mL of ammonium oleate surfactant was added to the paste, and sonicated for 3h using a 40 kHz bath sonicator before being incorporated into the cement mixtures [21]. The ammonium oleate surfactant was prepared by mixing 1 mL of oleic acid with 1 mL of concentrated ammonia solution and 50 mL of distilled water [21].

2.2. Preparations of nanomaterials modified cement paste

The G, GO, and BNNT particles in this study were first dispersed in water (Fig. 1) and then mixed with cement paste, which is convenient for mixing. These nanomaterials were incorporated into the cement mixture at 0.03 % by weight of cement content. The control mix (without nanomaterials) was prepared according to the mix proportions listed in Table 2. The water-to-cement ratio was kept constant at 0.35 for all mixes. This low water-to-cement ratio helped us focus on developing high-performance cement mixtures and enhancing the observable effects of nanomaterials on hydration and microstructure development. All mixing and sample preparation procedures were conducted at a controlled temperature of 23 °C ± 2 °C. This nanomaterial solution and the remaining water were then added to the dry contents of the cement and stirred for 180 s at 2000 rpm using an overhead stirrer. The mixing was completed in three steps: 1) 60 s of mixing, 2) 30 s rest, and 3) 90 s of mixing. The freshly prepared cement pastes were cast in a polyurethane tube and vibrated to remove entrapped air. The tube edges were sealed with bolts and clamped to prevent moisture loss. After demolding, the samples were stored in lime-saturated water at 23 °C until the specified testing age.

2.3. Materials characterization

2.3.1. Calorimetry

Isothermal calorimetry was used to study the in situ hydration

Table 1
Properties of nanomaterials used.

Properties	G (Graphene)	GO (Graphene Oxide)	BNNT
Composition	91%C; 7%O; 0.5% S; 2 % other elements	49-56%C; 41–50% O; 2–4%S; 0–2% other elements	>99%BN; 1 % elemental boron
Particle size	40 μm	<7 μm	Lengths up to 200 μm
Form Supplied	Dry Powder	Dispersion in water (4 mg/mL)	Dry Puffball
Surface area	–	–	Up to 400 m^2/g
Density	0.18 g/cm^3	–	Low tap density ~ 0.25 mg/cm^3
Structure	A single layer of carbon atoms arranged in a hexagonal lattice (up to 10 layers)	Oxidized graphene with various oxygen-containing groups disrupting the lattice (Single layer)	Network of isolated tubes and bundles (up to 5 tubes) 1–5 walls (2 or 3 most common)
Other properties			Extremely low defect density

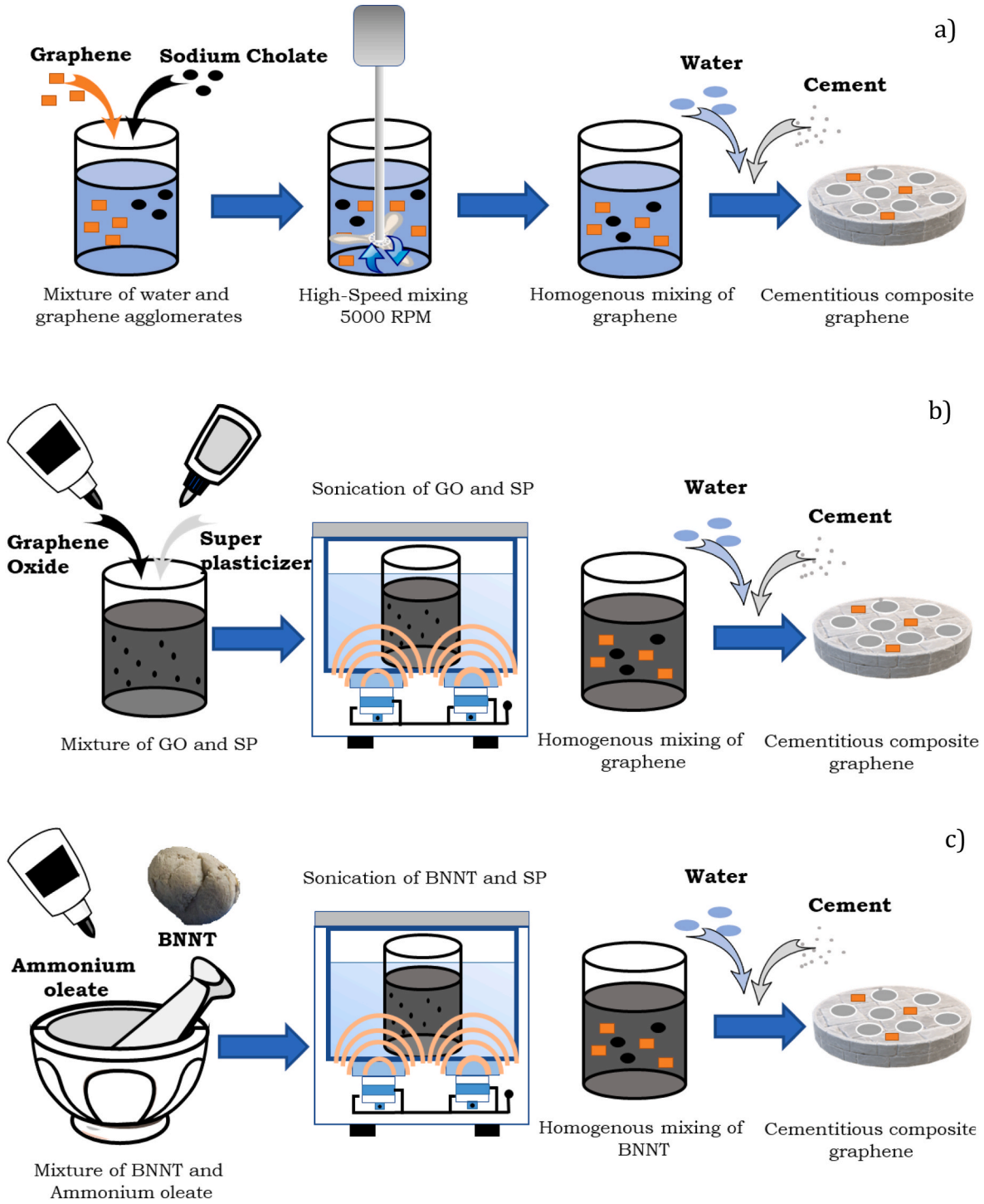

Fig. 1. Schematic presentation of methods used for the preparation of nanomaterials for cementitious composites: a) graphene-based, b) graphene oxide-based, c) BNNT.

Table 2
Mix contents of specimens in weight ratio.

S. No	Cement	Nanomaterial	Water	SP (wt of cement)	Surfactant
1	1	0	0.35	1 %	SP
2	1	G - 0.03 %	0.35	1 %	SP - sodium cholate
3	1	GO - 0.03 %	0.35	1 %	SP
4	1	BNNT - 0.03 %	0.35	1 %	SP - ammonium oleate

kinetics of cement paste. A thermometric air conduction calorimeter measured the heat flow. Freshly mixed pastes of approximately 7 g were cast into 25 mm diameter glass vials, resulting in a consistent sample thickness (5 mm). The vials were sealed and analyzed using a calorimeter for 168 h. A constant temperature of (23 ± 0.02 °C) was maintained in the measurement cells throughout the experiment. The hydration heat flow and cumulative hydration heat were normalized to the exact sample mass for each specimen. This normalization was performed to maintain consistency with standard calorimetry practices and to account for minor variations in sample mass, even though the intended cement

content was the same across all samples. This approach allows for more precise comparisons between samples within the study and facilitates easier comparison with results from other studies that may use different sample sizes.

2.3.2. Thermogravimetric analysis

Thermogravimetric analysis was used to assess the change in the phase composition of the cement pastes owing to hydration. For analysis, the cement pastes were cast into cylindrical plastic molds with an inner diameter of 5 mm. The cylinders were stored in a saturated aqueous solution of calcium at 23 ± 2 °C to prevent leaching. At designated ages, the specimens were ground, and hydration was halted by treatment with isopropanol and diethyl ether, followed by vacuum drying at 40 °C for 15 min. The treated samples were maintained under carbonation-free conditions until further testing. The thermogravimetric analysis was conducted up to 950 °C at a ramp rate of 5 °C/min. Thermogravimetric analysis was used to determine the calcium hydroxide (CH) content within the cement paste at different times and subsequently quantify the degree of evolution of hydration. TGA measurements were performed on days 1, 3, 7, and 28-day samples.

2.3.3. FTIR spectroscopy

Infrared spectroscopy reflects changes in the vibrational energy of molecules in a hydrated cement sample based on the location and shape of the absorption peak. The test is performed on the same sample used for TGA. In this study, the testing range of the wavenumbers used was 400–4000 cm^{-1}, which belongs to the middle-infrared region.

2.3.4. X-ray diffraction (XRD)

The nano-modified cement samples were analyzed using XRD to identify the mineral phases precipitated by the reaction. On a Bruker D8, Cu Kα radiation was used to collect XRD data with a 40 kV/40 mA advance diffractometer. For the measurements, a flat-plate Bragg-Brentano geometry incident beam and receiving Soller slits of 0.04 rad were used. A vertical goniometer with a 15 rpm spin was used to measure the particles over an angular range of 5°–70°2θ with a step size of 0.020°. The total measurement time per scan was 28 min, assuming a 0.50 s accumulated time per step. ZnO external standards were used to determine the amorphous content. XRF oxide composition and TGA measurements were used to calculate the mass absorption coefficient and bound water content.

2.3.5. ^{29}Si magic angle spinning nuclear magnetic resonance ^{29}Si MAS-NMR

Bruker Avance III HD 400 MHz NMR with silica probe was used to analyze finely ground hydration-stopped powdered samples. The sample is packed into a 4 mm zirconia O-ring rotor. 1D proton, 1D silicon, and ^{29}Si NMR spectra were recorded to identify the resonances. In NMR experiments, a sample is held in a magnetic field, and pulses of radio-frequency radiation are applied to cause nuclear spin to process, followed by the measurement of the electromagnetic response produced as the nuclei relax back to their equilibrium states. NMR spectra were analyzed to understand the structure and composition of the material, and comparisons were made with other characterization techniques, including X-ray diffraction, TGA, and electron microscopy, for a comprehensive understanding.

2.3.6. Scanning electron microscopy (SEM)

SEM images of the fracture surfaces of nano-modified cement were obtained using a scanning electron microscope. Hydration stoppage of the fracture samples was performed prior to testing. For hydration stoppage, the fracture samples were initially immersed in isopropanol for 30 min. The samples are then dried at 40 °C for 24 h. Prior to the SEM imaging, the fractured surfaces were sputter-coated with a thin layer (1 nm) of gold.

3. Results and discussions

This study focuses on the cement hydration process and microstructural development of cement with 0.03 BNNT, 0.03 GO, and 0.03 G on cement. In this study, a calorimetric analysis was performed on early age paste samples. TGA is performed on the 1-, 3-, 7-, and 28-day samples. The XRD, FTIR, NMR, and SEM analyses were conducted on samples taken at 7 and 28 days to assess the influence of nanomaterials on hydration and microstructure development.

3.1. Study of hydration

In situ calorimetry analysis provides a thermal profile that characterizes cement hydration. In this process, the relative rates of the different hydration reactions are compared. The detailed information on the maximum heat flow and the time of the peak's occurrence are listed in Table 3. The time taken for the sulfate depletion peak to occur was significantly reduced due to the incorporation of nanomaterials G, GO, and BNNT. Among these, the most pronounced reduction in time was observed with the use of BNNT. The acceleration effect of BNNT on the hydration process is evident in the occurrence of silicate and sulfate peaks. The silicate peak occurred at 12.5 h for BNNT, which was 19.5 %, 22.4 %, and 27.8 % earlier than that of GO, G, and the reference, respectively. Similarly, the sulfate peak appeared at 11.1 h for BNNT, 21.3 % earlier than GO, 24 % earlier than G, and 29.3 % earlier than the reference cement paste. These results demonstrate that the addition of BNNT into the cement mixture significantly accelerated the hydration process. The accelerated hydration observed with BNNT-modified cement could lead to faster construction, as this allows cement to gain strength more rapidly. This enables earlier formwork removal and quicker project completion, which leads to the cost savings and increased productivity in the construction industry. Additionally, higher early age strength development can enable the use of thinner structural elements or permit earlier load applications, leading to more efficient structural designs.

Calorimetry analysis of the compositions examined in this study revealed that the addition of BNNT, G, and GO nanomaterials reduced the induction period and induced the formation of C-S-H and CH at an earlier stage (Fig. 2(a)). Comparable results were observed by Wang et al. [22]. These results indicate that nanoparticles serve as heterogeneous nucleation sites for cement hydration products because of their large surface area. By increasing the reactive surface area, the energy barrier of the hydration reactions is reduced, resulting in improved kinetics, which in turn reduces the induction period. However, after approximately 40 h, the nanomaterials inhibited the hydration reaction, resulting in a slightly lower total heat flow, as shown in Fig. 2. This decrease is attributed to the higher density of the cement paste due to nanomaterials, which reduces the diffusion rate of reactant species. GO, in particular, creates a more effective physical barrier for reactant diffusion within cement paste due to its 2-D sheet-like structure and larger surface area.

Table 3
The heat flow and time at silicate peak and sulfate depletion peak occur with the addition of G, GO, and BNNT compared to plain cement modifications.

		Reference	0.03G	0.03GO	0.03 BNNT
Silicate peak	Maximum heat flow (mW/g)	4.33	4.35	4.6	4.57
	Time (h)	17.3	16.1	15.5	12.5
Sulfate depletion peak	Maximum heat flow (mW/g)	3.98	4.07	4.10	4.22
	Time (h)	15.7	14.6	14.1	11.1

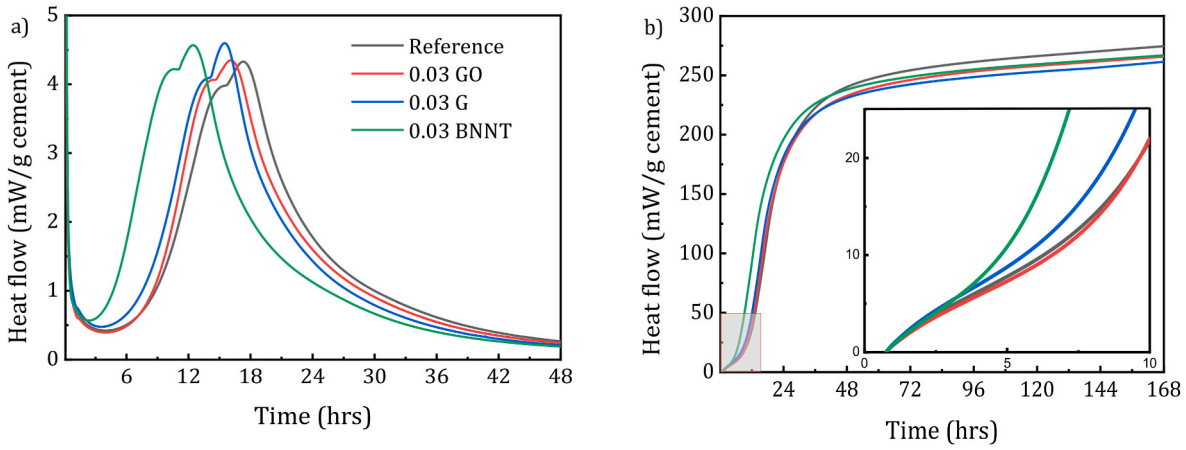

Fig. 2. Effect of BNNT, GO, and G on the hydration heat release of composite pastes during 48 h hydration: a) rate of heat of hydration over time, b) cumulative heat of hydration over time.

3.2. Thermogravimetric analysis (TGA)

The TGA shows an increase portlandite content with the nanomaterials. Fig. 3 shows the weight loss by TGA, a derivative of TG (DTG). As the temperature increases, the weight-loss percentage decreases gradually, and the DTG's inflections correspond to the specific phase of compound decomposition. The portlandite, $Ca(OH)_2$, was calculated as a measure of hydration of a corresponding hydrated cement composite. The endotherms and their corresponding mass losses in Fig. 4(a) are comparable to Bhojaraju et al. [4], and at the temperature of 30–105 °C, the evaporable water and part of the bound water escape. C-S-H, stratlingite C_2ASH_8, ettringite (Aft), Monosulphate(AFm_{ss}), mono-carbonate are altered at the temperature of 110–250 °C. Dehydroxylation of the $Ca(OH)_2$, i.e. CH at the temperature of 400–500 °C. At 650–800 °C decarbonation of calcium carbonate will take place. Hydration of cement composites is directly related to the CH content (CH%) Fig. 3 shows the mass loss by $Ca(OH)_2$ decomposition analysis. Overall, the CH content showed an increasing trend with the addition of nanocomposites. At 28 days, the 0.03BNNT composites resulted in a 5.4 % higher portlandite content than the 0.03G composites and a 13.0 % higher portlandite content than the 0.03GO composites. Compared to the control mix, BNNT showed an 18.5 % increase in portlandite content. Additionally, the degree of hydration for BNNT was 8.1 % higher than G, 16.9 % higher than GO, and 13.9 % higher than the control mix at 28 days, indicating its superior performance in enhancing cement properties. The CH content of 1, 3, 7, and 28 days (Fig. 3(b)) revealed that 0.03BNNT composites showed a higher degree of hydration than the other composites, followed by the 0.03G, 0.03GO, and control samples. After 24 h of hydration, both BNNT and G accelerated the cement composite hydration process, facilitating nucleation. Comparable trends were also observed in the calorimetric study.

Hydrophobic BNNT and G, as well as the presence of surfactants in the composition, may have contributed to the efficient hydration of the composite, which ultimately involved BNNT and G in the nucleation and growth stages of cement hydration. In contrast, GO's hydration rate is decreased for 1, 3, and 7 days, perhaps due to its hydrophilic nature, which absorbs water molecules from its surface and interlayer (Fig. 4). As a result, there is not enough water (w/c 0.35) to hydrate initially [23]. On the other hand, the hydration of cement modified with 0.03 GO increases after 28 days, which may be due to the reaction between the single bond COOH functional group and adjoining CH phases, leading to the formation of calcium carboaluminate hydrate [24]. The increased portlandite content observed with BNNT-modified cement, along with the increased degree of hydration and denser microstructure resulting from BNNT incorporation, can enhance concrete structures' durability and long-term performance, reducing maintenance costs and extending their service life.

3.3. FTIR spectroscopy investigation

Fig. 5 shows the infrared spectrum of all samples after 7 days and 28 days, with the spectrum ranging from 500 to 4000 cm^{-1}. The

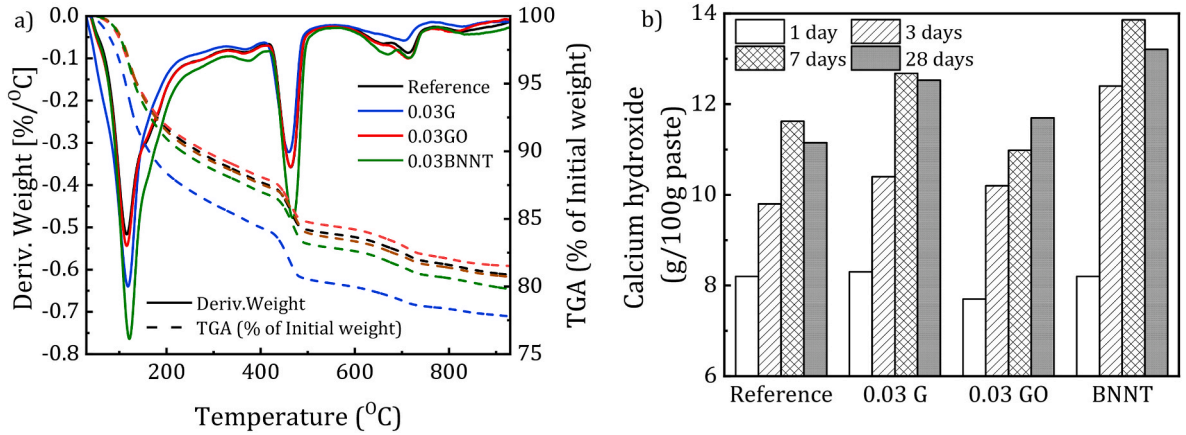

Fig. 3. Thermogravimetric analysis for nano modified cementitious composites: a) for different nanomaterials including G, GO, and BNNT, b) calcium hydroxide content.

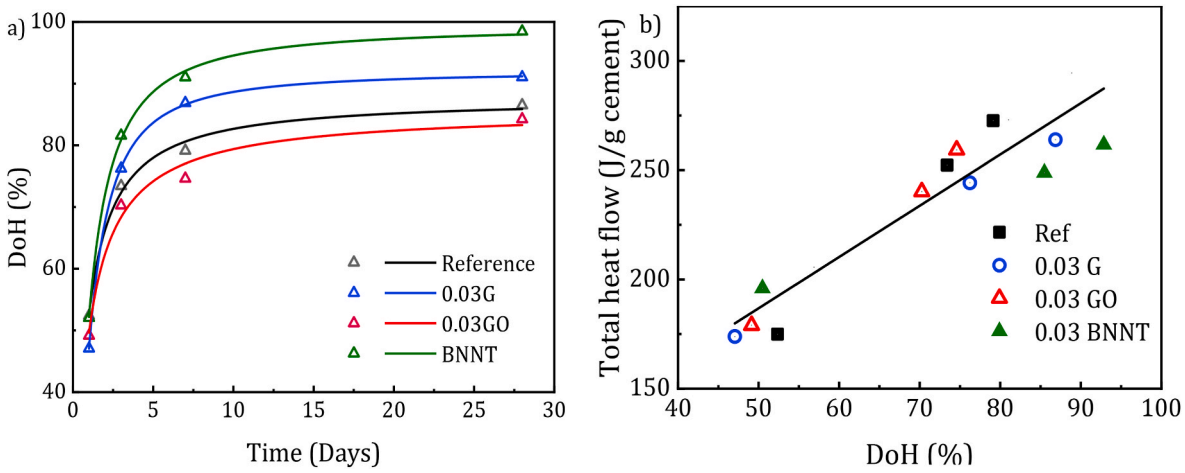

Fig. 4. Degree of hydration (a) and total heat flow (b) of the cement with nanomaterials.

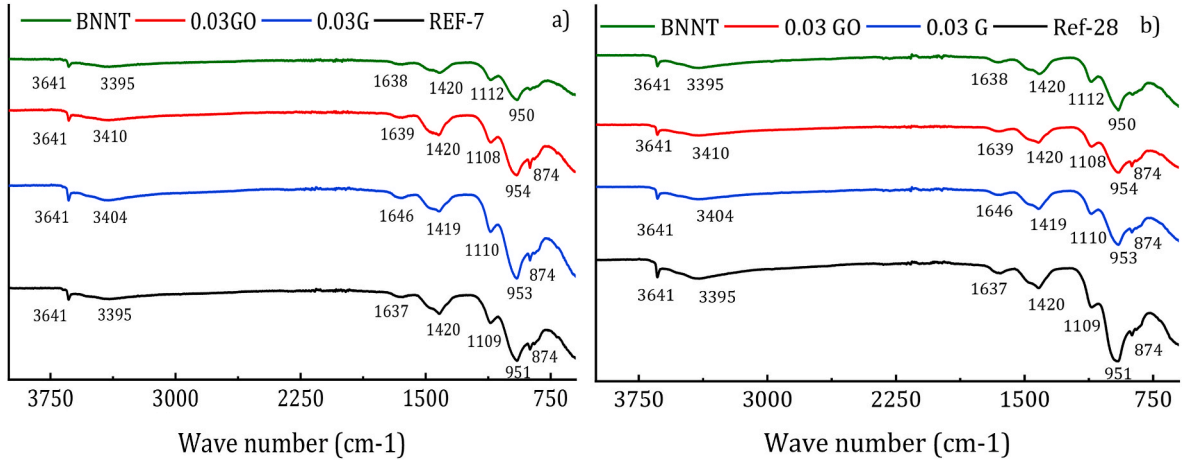

Fig. 5. FTIR Spectra of modified cement composites incorporating 0.03 % of G, GO, and BNNT a) 7 days and b) 28 days.

characteristic wavenumbers and the associated functional groups of Portland cement are listed in Table 4. The FTIR spectrum was obtained from the same powder samples as used in XRD and TGA tests. A slight peak in the vibrational band at 3641 cm^{-1} was also observed for BNNT, 0.03 GO, 0.03 G, and reference, which is related to the O–H bond in Ca $(OH)_2$ [25]. This observation is consistent with the XRD and TG results. The wide absorption band around 3400 cm^{-1} is caused by strong O-H stretching vibrations in water or hydroxyl groups [26]. The absorption in this range is stronger and wider in BNNT and 0.03GO samples compared to normal hydrated, and 0.03G sample. Furthermore, H-O–H bending vibration, representing chemically bonded water, shifts from 1637 cm to 1 in the reference sample to 1646 cm-1 in the 0.03G sample. This suggests that water is more weakly bonded with hydration products in 0.03G compared to BNNT and 0.03GO, a similar pattern is observed with Mollah et al. and Trezza, M [27,28]. An intense peak of vibration at 1404 to 1436 cm^{-1} corresponds to the symmetric stretching vibration of C-O or the asymmetric stretching of CO_2 ions [25]. The generated carbonates appear stable with all the mixtures [27,29]. For nano-modified cement, the stretching vibration of Si–O–Si (Si–O–Al) is evident in the 968–971 cm^{-1} region. Moreover, compared with the control, after the addition of these nanopowders, the absorption peak of Si–O–Si (Si–O–Al) shifts toward a higher wavenumber for G, GO, and BNNT, and it is predominant in BNNT samples. In cement, the chemical group that corresponds to the wave number at 951 cm^{-1} is known as the Si-O-Si stretching vibration. This vibration is unique to the silicon-oxygen-silicon bond found in the silicate minerals that form cementitious materials. The wave number at 950 cm^{-1} that is observed in BNNT is indicative of a particular vibration that is linked to the chemical structure of boron nitride. The wave numbers of 953 cm^{-1} and 954 cm^{-1} seen in 0.03GO and 0.03G, respectively, could indicate the presence of certain vibrations in the functional groups found in GO and G respectively. Further spectroscopic analysis would be needed to determine the exact functional groups or bonds responsible for these wave numbers. These observations suggest that the aluminum phase and silicon phase in the 0.03G and 0.03GO change the ratio of n(Ca)/n(Si) in C-S-H and form more C-S-H gels which leads to the enhancement of compressive strength. The absorption peak of $Ca(OH)_2$ decreases with the addition of the BNNT and 0.03GO, and the peak intensity is weakened due to the consumption of CH. This phenomenon is also observed in the results of the thermogravimetric and XRD analyses. The enhanced formation of CSH gels and reduced consumption of CH, potentially improves the durability of cementitious composites, aligning with sustainable construction practices.

Table 4
Wavenumber and its associated functional group.

Wavenumber (cm^{-1})	Functional Groups
968–971	Si–O–Si (Si–O–Al)
1400–1500	C–O (CO_3^{2-})
1400–1500	H_2O
1400–1500	H_2O
1400–1500	$Ca(OH)_2$

3.4. Hydration products formation

The typical cement hydration products are ettringite and portlandite (CH), tricalcium silicate (C_3S), and dicalcium silicate (C_2S), detected at all ages. XRD confirmed the phases of hydration indicated by TGA. The intensity of CH phases increases with 0.03BNNT and 0.03G in the composites and with age. The intensity of ettringite phases decreases with hydration age. However it increases in 0.03G composites. The crystalline phases also increase with the BNNT, G, and GO content. In order to quantify the amorphous C-S-H gel and other hydration products in the 28 days of hydrated composites, a quantitative analysis was performed using Rietveld analysis. The results are presented in Figs. 6 and 7. The calcite content increased with G, comparable to activated carbon and decolorized charcoal [30].

With the addition of 0.03 BNNT and 0.03 G, the portlandite and ettringite content increases. The increased formation of hydration products with BNNT contributes significantly to construction sustainability. By enhancing the cement's microstructure, BNNT may increase the material's strength and durability, potentially leading to long-lasting structures that require less maintenance over time.

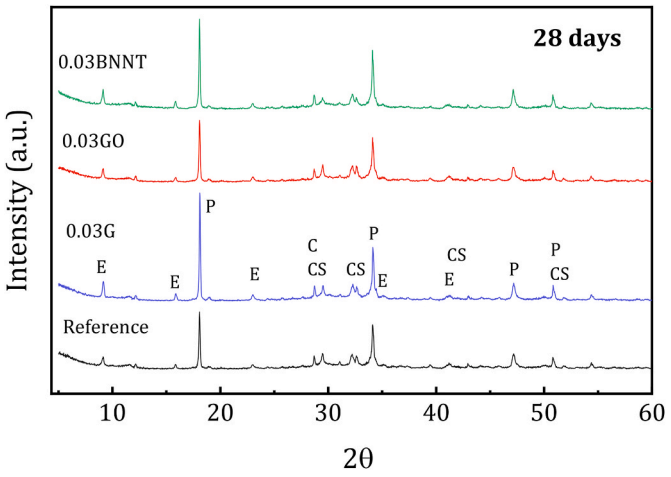

Fig. 7. XRD patterns of the nano-modified cement composites at 28 days (P; Portlandite, C; Calcite, E; Ettringite, CS).

3.5. ^{29}Si MAS-NMR analysis

A^{29}Si MAS NMR study investigates the influence of the nanomaterials on the microstructure of C-S-H. Tobermorite-like structures are generally accepted for the C-S-H phase, which typically includes layers of CaO_2 with seven coordinated Ca^{2+} ions, where oxygen atoms are shared between Si^{4+} tetrahedra chains. The spectrum of the silicate anion falls within the range of 70–76 ppm for Q_0, 78 for Q_1, and 82.8 for Q_2, as shown in Fig. 8. The Q_0 sites correspond to the C_3S content or dehydrated cement, Q_1 represents the end-chain silicate tetrahedral, whereas Q_2 represents the middle chain silicate tetrahedron with two neighbouring Q_1 sites. The middle chain silicate can be bound either to a three-Ketten position (Q_2b) or to a proton (Q_2p) [31]. Quantitative results are obtained by deconvolution of the superimposed NMR signals. Table 5 presents the deconvolution results of cement pastes at various hydration ages and their decalcification samples. A Gaussian function was used to fit the deconvolution of the experimental data of each silicate anion. In the C-S-H, the mean chain length (MCL) is calculated using Richardson's equation.

A^{29}Si-NMR spectrum of samples after 7 and 28 days of curing time is shown in Fig. 8, and the deconvolution information is shown in Table 5. The hydration degrees are quantitatively obtained using the Q_0 area. After 7 days, these values are 62.7 %, 66.3 %, 55.8 %, and 75.6 % for normal concrete, 0.03G, 0.03GO, and 0.03BNNT samples, respectively. After 28 days, the values increase to 70.4 %, 70.0 %, 67.5 %, and 78.3 %, respectively. The hydration degree is highest for 0.03BNNT addition, followed by 0.03G. Interestingly, for 0.03GO, the hydration rate is very low, and these results do not agree with TGA and XRD measurements. NMR can detect molecular interactions in specific areas, so it may show that GO has less water interaction because of its complex surface chemistry or structural aspects. Meanwhile, other methods explore hydration in a more comprehensive way by considering surface chemistry, functional groups, crystallinity, and the accessibility of water to nanomaterials. From the literature, it was observed that the elongation of the mean chain lengths and packing of the chains could stiffen the material and improve its mechanical performance [32,33]. The maximum chain length was observed for BNNT, possibly due to alteration of the CSH structure. Interestingly, the chain for normal cement is reducing with time (28 days). G and GO reacted chemically with carboxylic compounds, and these could not change the structure of C-S-H. The elongated C-S-H chain length observed with the addition of BNNT could enhance the sustainability of construction materials. This could result in long-lasting structures with reduced maintenance needs, decreasing the environmental impact over time.

3.6. Morphological characterization

Fig. 9 depicts the interfacial microstructures of the specimens for reference, 0.03G, 0.03GO, and 0.03BNNT after 7 days. All four images have the same magnification factor. The plain cement paste sample (Fig. 9(a)) displays clear cracks that penetrate through the dense

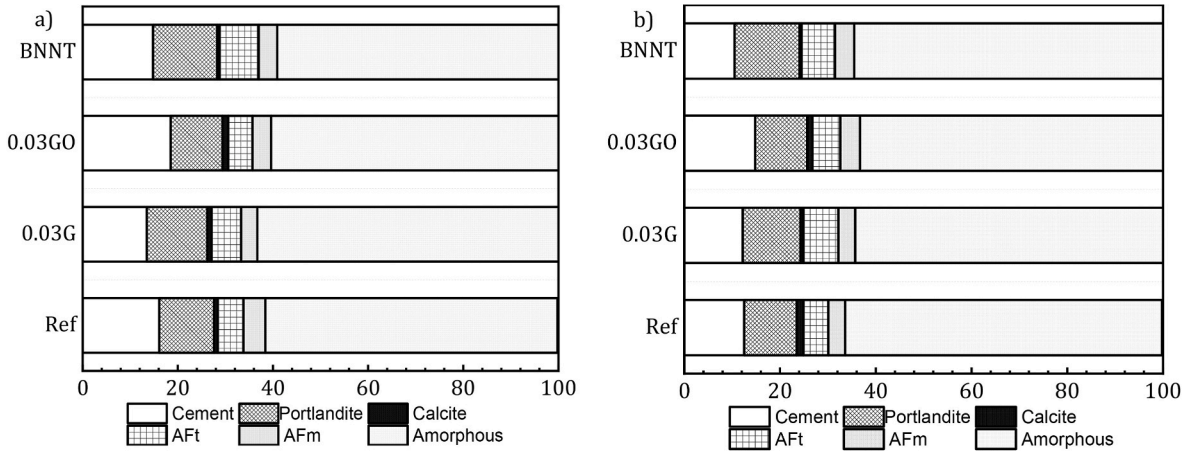

Fig. 6. Mixes composition of various nano-modified cementitious composites after solvent exchange hydration stoppages for A) 7 and B) 14 days.

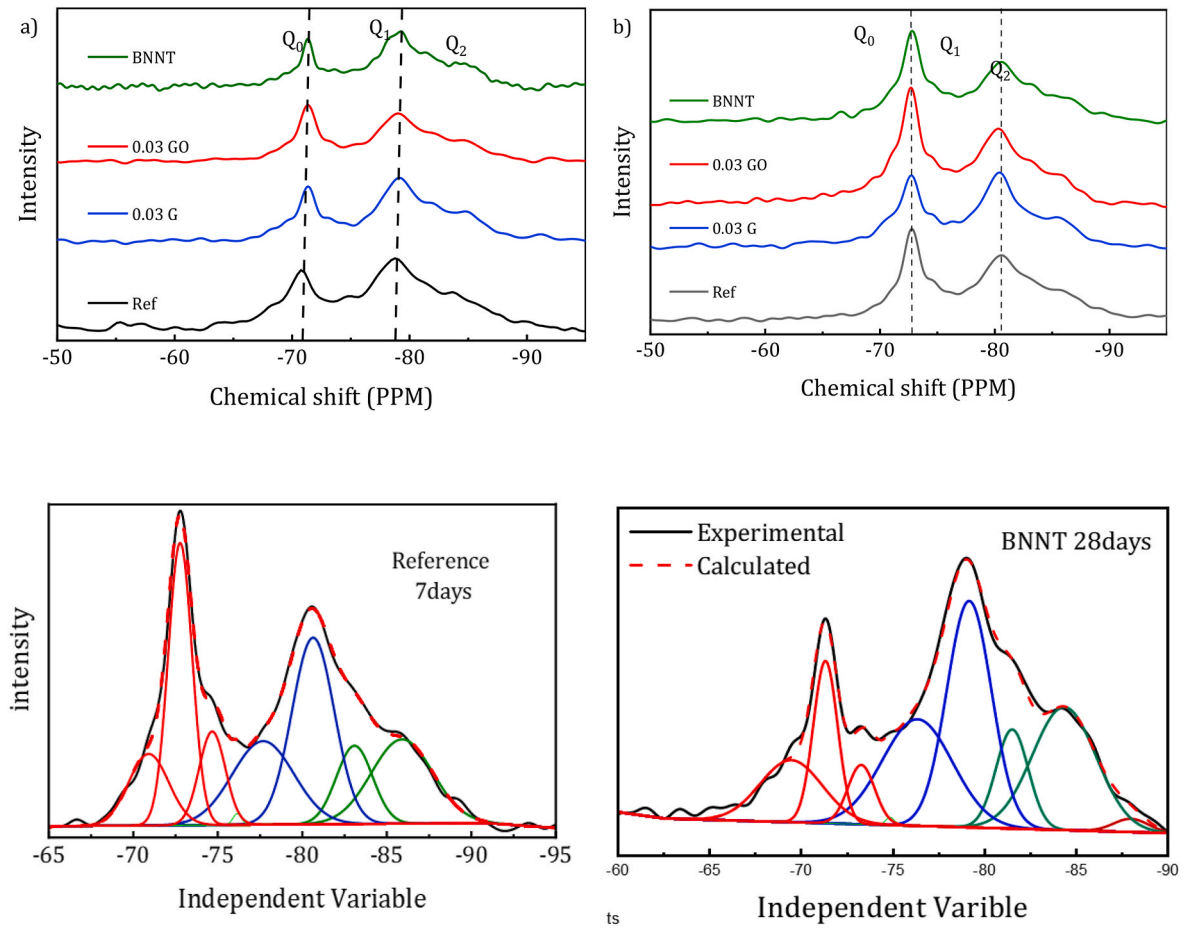

Fig. 8. 29 Si NMR spectra of nano-modified cementitious composite a) 7 days, b) 28 days, c) Simulated spectra of 7 days GO d) Simulated spectra of 28 days. The black line represents experimental values. Red, blue, and green color lines represented the Gaussian deconvolution of Q_0, Q_1, and Q_2 peaks, respectively. Finally, the red dashed line indicated the fitting values of the convolutions. (For interpretation of the references to color in this figure legend, the reader is referred to the Web version of this article.)

Table 5
Percentages of silicate chemical shift from 29Si-NMR spectra for 7 and 28 days.

7 days	Q0	Q1	Q2	MCL
Reference	29.65	46.05	21.75	2.94
0.03G	29.99	43.29	26.72	3.39
0.03GO	32.49	44.36	23.16	3.04
BNNT	21.75	43.99	34.26	3.56
28 days				
Reference	37.32	38.66	24.03	3.24
0.03G	33.75	44.76	21.49	2.96
0.03GO	44.24	46.24	9.52	2.41
BNNT	24.37	45.81	29.82	3.30

hydration products. Fig. 9 demonstrates the effective dispersion of nanofillers in the hardened cement paste. Compared to the control specimens, more hydration products are attached to the surface of nanoparticles, and the morphology of hydration products is consistent throughout the cement paste matrix for nano-modified composites. Fig. 9(b) shows a predominant two-dimensional structure in graphene nanoplatelets. Each layer is stacked and connected to the next. Fig. 9 shows SEM micrographs of nano-modified pastes with the same morphological characteristics. As shown in Figs. 9(c), 0.03 wt% GO significantly enhances the structure of the hardened cement paste. The resulting C-S-H gel exhibits improved uniformity and compactness, forming a well-organized layer over other crystals and cement particles [34]. GO sheets stand out among other nanofillers due to their distinctive two-dimensional structure, which can redirect cracks, causing them to deviate or curve in their path. The images demonstrate that the mixing method adopted during the experiment did not damage the nano inclusions. There are less recognizable particles of BNNT and GO in the cement matrix. However, the nanofillers examined in the research resulted in acceptable dispersion of particles in cementitious materials, since they did not aggregate into bulky bundles. The incorporation of nano-BNNT results in a densely packed C-S-H gel structure. As shown in Fig. 9(d), plenty of C-S-H gel-wrapped nano-BNNT is found in the void of CH crystal, which limits the growth of CH crystals and then reduces the size and orientation of CH crystals [35].

While the study provided valuable insights into the hydration behavior of cement composites incorporating nanomaterials (BNNT, G, and GO), certain limitations should be acknowledged. In the present investigation, we focused on a 0.35 w/c ratio and a single dosage of nanomaterials, disregarding the potential impact of varying these proportions. Furthermore, this study mainly focused on early age hydration (up to 28 days), and other aspects, including long-term microstructural alterations and durability, were not considered. Additionally, no mechanical tests were conducted to evaluate the impact of nanomaterials. It is essential to acknowledge that this study is conducted on a laboratory scale and may not represent a large-scale application. Moreover, although we utilized advanced analytical techniques, each method has limitations in terms of resolution, detection limits, and sample preparation requirements, which could impact the interpretation of results. Thus, future research should consider the influence of varying w/c ratio and dosage of nanomaterials on hydration and mechanical properties. In

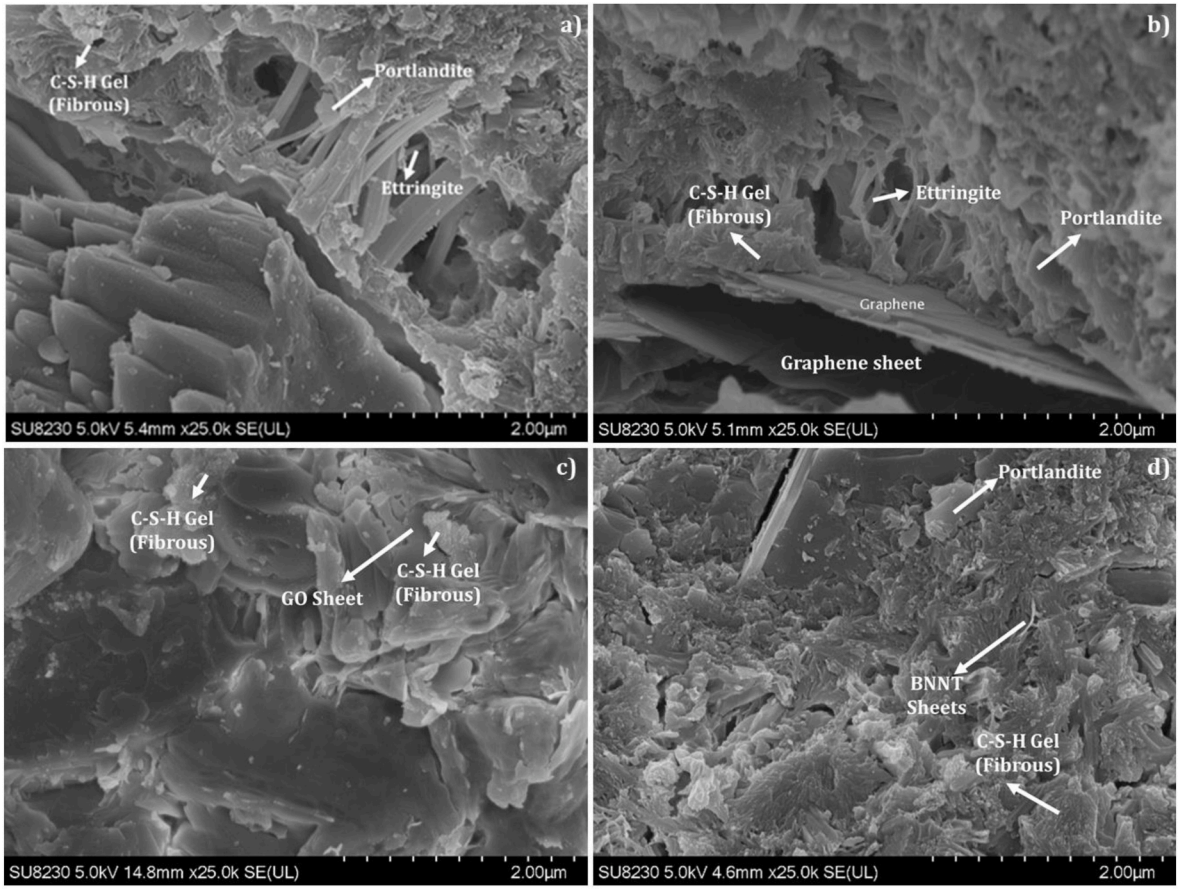

Fig. 9. SEM images of cement paste at 7 days: a) reference cement, b) cement with graphene, c) cement with graphene oxide, and d) cement with BNNT modified.

addition, the investigation of long-term performance is essential for practical applications. The synergistic effect of combining these nanomaterials can be investigated, potentially this may lead to novel, high-performance cement composites. Finally, the opportunity for scaling up production and economic viability for practical applications in the construction industry should be explored.

4. Conclusion

The use of nanomaterials in cementitious composites offers a promising avenue for enhancing their performance. As part of this investigation, an experimental program was conducted to study the effect of nanomaterials (BNNT, G, GO) on the hydration behavior, phase development, and degree of hydration of cement composites. Advanced analytical techniques, including isothermal calorimetry, TGA, FTIR spectroscopy, XRD analysis, 29SI-NMR, and SEM, were used. The analysis of the results yields the following conclusions.

- Generally, the addition of nanomaterials increases heat generation during hydration and accelerates the reaction rate due to the nucleation effect. Specifically, BNNT accelerates the occurrence of the silicate peak by 27.8 % and the sulfate peak by 29.3 % compared to the reference. Composites with BNNT show significant acceleration compared to other nanomaterials.
- TGA results of cementitious composites indicate that the presence of nanomaterials enhances CH content, with BNNT having the maximum value, followed by G. 0.03BNNT exhibits a higher degree of hydration throughout all ages. At 28 days, 0.03 % BNNT-modified composites show an 18.5 % increase in portlandite content, and a 13.9 % higher degree of hydration compared to the reference.
- XRD analysis reveals that the addition of BNNT and G to nano-modified cementitious composites significantly increases portlandite and ettringite content while drastically reducing unreacted cement content, even at an early age of 7 days. However, for 0.03GO, the portlandite peak decreases while calcite content increases. Compared to 0.03GO and cement, 0.03BNNT exhibits a significantly higher degree of hydration at 28 days. BNNT addition causes a progressive shift in O-Si-O stretching vibration, indicating a high degree of hydration and characteristic enhancements.
- ^{29}Si MAS NMR determines the extent of hydration to be 62.7 %, 66.3 %, 55.8 %, and 75.6 % at 7 days for cement, 0.03G, 0.03GO, and 0.03BNNT, respectively. 0.03BNNT shows a significantly higher degree of hydration compared to other nanomaterials (G and GO) and the reference sample. This trend persists for 28 days. The mean silicate chain length (MCL) of the C-S-H gel is estimated to be 2.97 for the reference cement at 7 days, increasing to 3.56 with the addition of BNNT. This trend of superior hydration for BNNT is consistently observed for 1, 3, 7, and 28 days.
- SEM images show that for lower dosages of GO and BNNT with the current dispersion methods, no agglomeration is observed in the microstructure of the composites. These nanomaterials increase cementitious matrix density. The improved microstructure, combined with accelerated hydration kinetics and enhanced CH content, confirms that BNNT has significant potential for improving early-age strength development and long-term durability of cementitious composites.

CRediT authorship contribution statement

Chandrasekhar Bhojaraju: Writing – original draft, Visualization, Validation, Methodology, Investigation, Formal analysis, Data curation.

Claudiane M. Ouellet-Plamondon: Writing – review & editing, Writing – original draft, Validation, Supervision, Resources, Project administration, Methodology, Funding acquisition, Formal analysis, Data curation, Conceptualization.

Declaration of competing interest

The authors declare that they have no known competing financial interests or personal relationships that could have appeared to influence the work reported in this paper.

Acknowledgement

The research was supported by NSERC Discovery programs (RGPIN-2016-5011 and RGPIN-2023-05505) and FRQNT Quebec Centre for Advanced Materials (QCAM). Dr Victor Brial is thanked for the Rietveld analysis of the XRD results.

Data availability

Data will be made available on request.

References

[1] G. Habert, et al., Environmental impacts and decarbonization strategies in the cement and concrete industries, Nat. Rev. Earth Environ. 1 (11) (2020) 559–573.
[2] A.C.A. Muller, et al., Use of bench-top NMR to measure the density, composition and desorption isotherm of C–S–H in cement paste, Microporous Mesoporous Mater. 178 (2013) 99–103.
[3] P.J. Monteiro, et al., Advances in characterizing and understanding the microstructure of cementitious materials, Cement Concr. Res. 124 (2019) 105806.
[4] C. Bhojaraju, M. Di Mare, C.M. Ouellet-Plamondon, The impact of carbon-based nanomaterial additions on the hydration reactions and kinetics of GGBS-modified cements, Construct. Build. Mater. 303 (2021) 124366.
[5] W. Meng, K.H. Khayat, Effect of graphite nanoplatelets and carbon nanofibers on rheology, hydration, shrinkage, mechanical properties, and microstructure of UHPC, Cement Concr. Res. 105 (2018) 64–71.
[6] C. Bhojaraju, S.S. Mousavi, C.M. Ouellet-Plamondon, Influence of GGBFS on corrosion resistance of cementitious composites containing graphene and graphene oxide, Cement Concr. Compos. (2022) 104836.
[7] A.P. Lange, et al., Mass transport in binary TiO2: SiO2 and GeO2: SiO2 direct ink write glasses, J. Am. Ceram. Soc. 105 (7) (2022) 4681–4690.
[8] S.V. Anandhan, U.M. Krishnan, Boron nitride nanotube scaffolds: emergence of a new era in regenerative medicine, Biomed. Mater. 16 (4) (2021) 044105.
[9] J.V. Rau, et al., Tricalcium phosphate cement supplemented with boron nitride nanotubes with enhanced biological properties, Mater. Sci. Eng. C 114 (2020) 111044.
[10] A. Falin, et al., Mechanical properties of atomically thin boron nitride and the role of interlayer interactions, Nat. Commun. 8 (1) (2017) 15815.
[11] Q. Weng, et al., Functionalized hexagonal boron nitride nanomaterials: emerging properties and applications, Chem. Soc. Rev. 45 (14) (2016) 3989–4012.
[12] R. Shahsavari, Intercalated hexagonal boron nitride/silicates as bilayer multifunctional ceramics, ACS Appl. Mater. Interfaces 10 (3) (2018) 2203–2209.
[13] A.L. Tamilkovan, P. Arumugam, A current review on boron nitride nanotubes and their applications, Adv. Nat. Sci. Nanosci. Nanotechnol. 15 (1) (2024) 013002.
[14] A.G. Pornea, et al., Preparations and thermal properties of PDMS-AlN-Al2O3 composites through the incorporation of poly (Catechol-Amine)-Modified boron nitride nanotubes, Nanomaterials 14 (10) (2024) 847.
[15] R.K. Ameta, et al., Hexagonal boron nitride for bone tissue engineering application, in: Hexagonal Boron Nitride, Elsevier, 2024, pp. 321–350.
[16] F.W. Degrazia, et al., Boron nitride nanotubes as novel fillers for improving the properties of dental adhesives, J. Dent. 62 (2017) 85–90.
[17] M.A. Rafiee, et al., Hexagonal boron nitride and graphite oxide reinforced multifunctional porous cement composites, Adv. Funct. Mater. 23 (45) (2013) 5624–5630.
[18] J. Liu, W. Jian, D. Lau, Boron nitride nanosheet as a promising reinforcement for cementitious composites, Appl. Surf. Sci. 572 (2022) 151395.
[19] D. Dimov, et al., Ultrahigh performance nanoengineered graphene–concrete composites for multifunctional applications, Adv. Funct. Mater. 28 (23) (2018) 1705183.
[20] S. Chuah, et al., Investigation on dispersion of graphene oxide in cement composite using different surfactant treatments, Construct. Build. Mater. 161 (2018) 519–527.
[21] J. Yu, Y. Chen, B.-M. Cheng, Dispersion of boron nitride nanotubes in aqueous solution with the help of ionic surfactants, Solid State Commun. 149 (19–20) (2009) 763–766.
[22] W. Wang, et al., Exfoliation and dispersion of boron nitride nanosheets to enhance ordinary Portland cement paste, Nanoscale 10 (3) (2018) 1004–1014.
[23] F. Babak, et al., Preparation and mechanical properties of graphene oxide: cement nanocomposites, Sci. World J. 2014 (2014).
[24] M. Mokhtar, et al., Mechanical performance, pore structure and micro-structural characteristics of graphene oxide nano platelets reinforced cement, Construct. Build. Mater. 138 (2017) 333–339.
[25] R. Ylmén, et al., Early hydration and setting of Portland cement monitored by IR, SEM and Vicat techniques, Cement Concr. Res. 39 (5) (2009) 433–439.
[26] P. Yu, et al., Structure of calcium silicate hydrate (C-S-H): near-, Mid-, and Far-infrared spectroscopy, J. Am. Ceram. Soc. 82 (3) (1999) 742–748.
[27] M.Y. Mollah, M. Kesmez, D.L. Cocke, An X-ray diffraction (XRD) and Fourier transform infrared spectroscopic (FT-IR) investigation of the long-term effect on the solidification/stabilization (S/S) of arsenic (V) in Portland cement type-V, Sci. Total Environ. 325 (1–3) (2004) 255–262.
[28] M. Trezza, A. Lavat, Analysis of the system 3CaO· Al2O3–CaSO4· 2H2O–CaCO3–H2O by FT-IR spectroscopy, Cement Concr. Res. 31 (6) (2001) 869–872.
[29] R. Hanna, et al., Solid state 29Si and 27Al NMR and FTIR study of cement pastes containing industrial wastes and organics, Cement Concr. Res. 25 (7) (1995) 1435–1444.
[30] V. Brial, T. Duplessis, C.M. Ouellet-Plamondon, Accelerating effect of low replacements of carbonaceous materials in cement paste and mortar, CEMENT 18 (2024) 100118.
[31] B. Walkley, J. Provis, Solid-state nuclear magnetic resonance spectroscopy of cements, Mat. Today Adv. 1 (2019) 100007.
[32] D. Hou, J. Yu, P. Wang, Molecular dynamics modeling of the structure, dynamics, energetics and mechanical properties of cement-polymer nanocomposite, Compos. B Eng. 162 (2019) 433–444.
[33] H. Yang, et al., Experimental study of the effects of graphene oxide on microstructure and properties of cement paste composite, Compos. Appl. Sci. Manuf. 102 (2017) 263–272.
[34] H. Peng, et al., Mechanical properties and microstructure of graphene oxide cement-based composites, Construct. Build. Mater. 194 (2019) 102–109.
[35] X. Wang, et al., Effect and mechanisms of nanomaterials on interface between aggregates and cement mortars, Construct. Build. Mater. 240 (2020) 117942.